

## **RECENT DEVELOPMENTS OF TiAl ALLOYS TOWARDS IMPROVED HIGH-TEMPERATURE CAPABILITY**

F. Appel<sup>a</sup>, J.D.H. Paul<sup>a</sup>, M. Oehring<sup>a</sup>, C. Buque<sup>a</sup>, Ch. Klinkenberg<sup>b</sup>, and  
T. Carneiro<sup>c</sup>

<sup>a</sup> Institute for Materials Research, GKSS Research Centre Geesthacht, D-21502 Geesthacht  
Germany

<sup>b</sup> Niobium Products Company GmbH, Steinstrasse 28, 40210 Düsseldorf, Germany

<sup>c</sup> Reference Metals Company, Inc. 1000 Old Pond Road, Bridgeville, PA 15017-0217, USA

Keywords: Titanium Aluminides, Hot-Working, Investment Casting, Creep

### **Abstract**

Titanium aluminide alloys based on relatively large Nb additions, together with fine dispersions of precipitates, exhibit attractive thermo-physical properties, which extend the service range of conventional TiAl alloys. Engineering alloys can be tailored for strength, toughness, creep resistance, and environmental stability. These concerns are addressed in the present paper through a global commentary on the physical metallurgy and the associated processing technologies.

### **Introduction**

Demands for higher strength coupled with good oxidation resistance have led to the development of a new family of  $\gamma$ (TiAl) alloys with the base-line composition (at.%)

Ti-45Al-(5-10)Nb+X, (1)

with X designating modest amounts of several other metallic and non-metallic elements [1-3]. Optimized alloys have been identified that are capable of carrying stresses of 700 MPa at a service temperatures around 700 °C. The alloys exhibit at room temperature yield stresses in excess of 1 GPa combined with plastic tensile elongations of about 2%. Thus, alloys of this type extend the service range of conventional TiAl alloys and can be an attractive alternative to the heavier nickel-base superalloys in certain ranges of stress and temperature. However, in order to use the materials at their full potential, structural and chemical consolidation are major concerns. Nevertheless, information about processing and mechanical properties is still limited. This lack of knowledge is addressed in the present paper through a discussion of the physical metallurgy of this novel class of TiAl alloys and the associated mechanical properties. The major areas of the study are (i) hot-working based on ingot metallurgy, (ii) investment casting, (iii) mechanical properties.

### **Design Criteria**

The characteristic feature of the new alloys described by the general composition (1) is the low Al content combined with high Nb additions. The strengthening of Nb-bearing alloys apparently becomes significant for Nb contents higher than 5 at. % [1-6]. Atom location by

channelling enhanced microanalysis (ALCHEMI) studies have revealed that Nb solely occupies the Ti sublattice [7]. There is only a small size misfit between Ti and Nb atoms of about 0.2% [8], which seems unlikely to completely explain the observed strengthening effect in Al-lean alloys. This viewpoint was confirmed by analyzing thermodynamic glide parameters, such as activation volume and activation energy [1,2]. For Ti-Al systems that are of technical significance, alloying with Nb generally decreases the  $\beta$ (B2)- and  $\alpha$ -transus temperatures and contracts the  $\alpha$  phase field [6]. This modification of the phase stabilities leads to a significant structural refinement, which was confirmed by electron microscope observations [1,2] and is undoubtedly the most important source of the high yield strength of the material [1-3]. In high

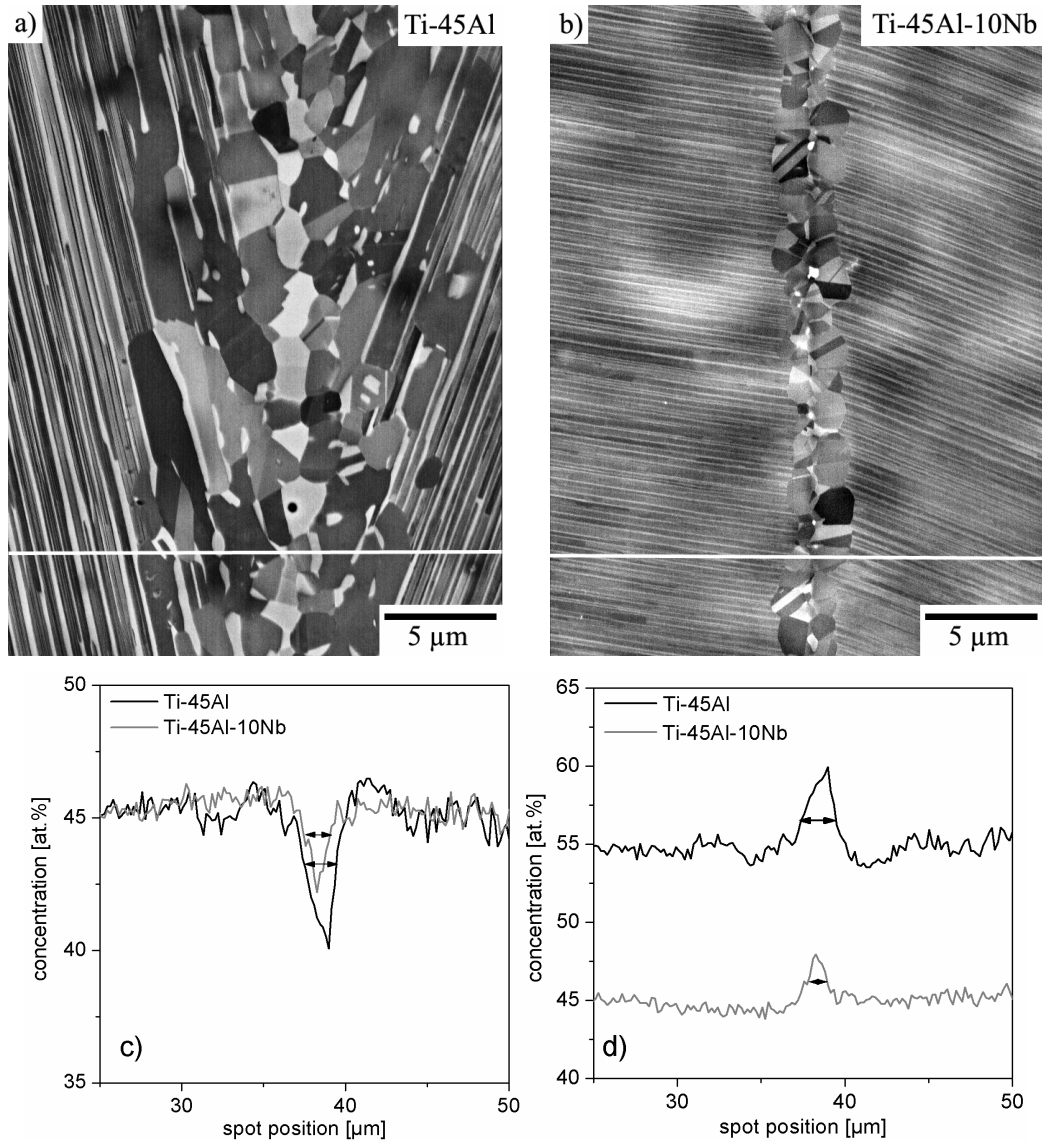


Fig. 1: Recrystallization and diffusion characteristics of binary and Nb-bearing alloys. Microstructure and phase distribution at the bonding interfaces of diffusion couples. Diffusion bonding in vacuum at 950 °C, stress  $\sigma=60$  MPa for 2 hours. Scanning electron micrographs taken in the back-scattering electron mode (BSE). (a) Ti-45Al; (b) Ti-45Al-10Nb. (c, d) Quantitative EDX analysis of the Al and Ti concentration across the bonding zone as indicated in (a) and (b) by the white lines. Note for the Nb-bearing alloy the significantly smaller diffusion zone, the lesser amount of  $\alpha_2$  phase, and the high density of annealing twins in recrystallized  $\gamma$  grains.

Nb containing alloys an abundant activation of mechanical twinning has been recognized, which suggests that the stacking fault energy is changed by Nb additions [1]. It is tempting to speculate that the enhanced twinning activity in Nb-bearing alloys is beneficial for the low-temperature ductility, in that it compensates for the lack of independent slip systems in  $\gamma$ (TiAl) that can operate at comparable stresses [9].

Concerning high-temperature strength and creep resistance, the important point to note is that the activation enthalpy for thermally activated deformation is significantly higher when compared with conventional alloys [1-3]. The values for conventional alloys determined at  $T=1100$  K are  $\Delta H=2.9-3.2$  eV, while high Nb containing alloys represented by the general composition (1) exhibit enthalpies of  $\Delta H=4.19-4.46$  eV. This finding agrees with recent radio tracer measurements of the Nb solute diffusion, which revealed that Nb is a slow diffuser in  $\gamma$ (TiAl) [10]. This result implies that diffusion-assisted transport processes might be impeded in such alloys, which is an important prerequisite for good high-temperature strength and oxidation resistance.

The deformation characteristics described here were deduced from detailed electron microscope observations and the analysis of thermodynamic glide parameters [1-3]. Direct evidence was also obtained from recent studies of diffusion bonding; this reflects the characteristics of deformation and diffusion in a comprehensive manner [11,12]. Figure 1 demonstrates the structural details in the bonding zones of diffusion couples of a binary Ti-45Al and a high Nb containing alloy Ti-45Al-10Nb. The Nb-bearing alloy exhibits a significantly higher density of annealing twins in the recrystallized  $\gamma$  grains of the diffusion zone, which indicates that the stacking fault energy is reduced. The lower diffusibility of this material is directly manifested in the lower width of the diffusion zone, when compared with the binary reference material (Fig. 1c).

The Nb-bearing alloys investigated here were subjected to precipitation reactions, in order to improve high-temperature strength and creep resistance and to stabilize the microstructure. Boron was added as a grain refining coagulant in order to retard grain growth in the high-temperature  $\alpha$  and  $\beta$  phase fields. The alloy performance critically depends on the size and the dispersion of the particles. In this respect, carbides, nitrides and silicides appear beneficial, as the optimum dispersion can be achieved by homogenization and ageing procedures. From conventional alloys it is quite clear that hardening of the matrix alone is not necessarily a source of great strength, but is only one of many factors that have to be considered as contributing to the resistance to deformation. For high-Nb containing alloys stabilization of the very fine microstructure is probably equally important. This can be achieved by adapting alloy chemistry and processing so that the precipitates are preferentially nucleated at the mismatch structures of newly formed internal boundaries. With this perspective in mind, hot-working operations have been successfully applied and combined with precipitation reactions. From the engineering point of view, the challenge was to establish the precipitation reactions without compromising desirable low-temperature properties such as ductility and toughness. In this optimisation procedure, in particular, the effects of Nb, B, C, and elements stabilizing the  $\beta$  phase were harmonized; this resulted in the definition of engineering alloys designated as TNB, which will be specified for the examples given.

## Hot-Working Based on Ingot Metallurgy

The feasibility of wrought processing of TNB alloys was systematically studied by mechanical testing and metallographic inspection. As with conventional TiAl alloys, hot-working can be performed in the  $\alpha$  field, which results in refined fully lamellar microstructures. The colony size is essentially determined by dynamic recrystallization of the  $\alpha$  phase, from which the

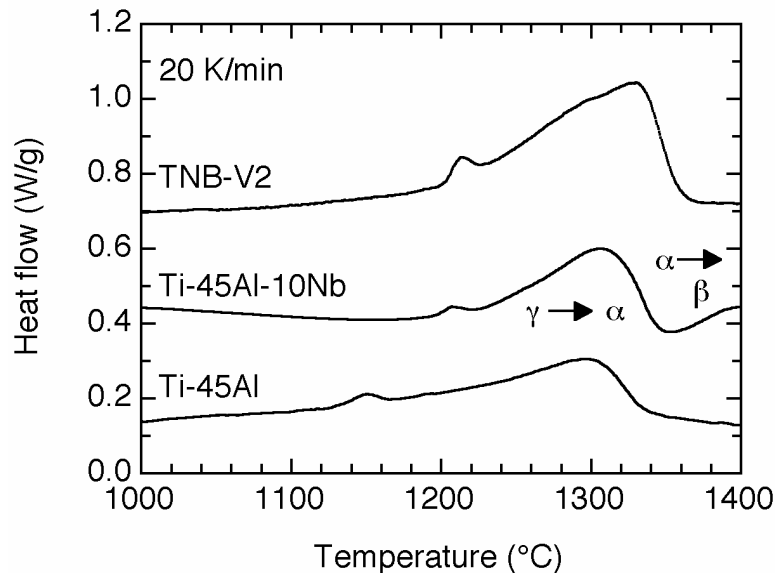


Fig. 2: Effects of Nb additions on phase transformations. DSC traces obtained from a binary and high Nb containing alloys on heating the specimen with 20 K/min. By extrapolating of the peaks in heat flow, the eutectoid,  $\alpha$ -transus and  $\alpha/\alpha+\beta$  transition temperatures were determined. To make these plots readable, the curve belonging to Ti-45Al-10Nb was shifted along the ordinate.

colonies are formed. Hot-working can also be performed below the  $\alpha$ -transus temperature  $T_{\alpha}$ , which results in fine equiaxed or duplex microstructures. Figure 2 shows traces of differential scanning calorimetry (heat flux DSC) of a Ti-45Al-10Nb alloy and the equivalent binary Ti-45Al alloy, from which the relevant phase transition temperatures can be deduced.

The range of potential temperatures and strain rates for hot-working operations was evaluated through compression testing of cylinders with volumes of a few cubic centimeters followed by metallographic inspection. Forging operations of as-cast material can be carried-out near the eutectoid temperature with strain rates up to  $10^{-2} \text{ s}^{-1}$ . The flow stress response observed in this domain reflects the effect of dynamic recrystallization in that the flow curves exhibit a broad peak at low strains ( $\epsilon \approx 10\%$ ), followed by flow softening to an ostensibly constant stress level at  $\epsilon = 60-80\%$  (Fig. 3a).

Metallographic inspection and comparison with a binary Ti-47Al alloy have shown that dynamic recrystallization and globularisation of the microstructure seem to be retarded by high Nb additions, which may be due to at least three factors. Nb is known to occupy exclusively the Ti sites in the  $\alpha_2$  and  $\gamma$  phase [7]. Thus, the Nb bearing alloys considered here are equivalent to Ti-45Al. In such Ti-rich alloys, dynamic recrystallization is generally sluggish because strain localization in shear bands occurs [13]. It might also be speculated that recrystallization is

retarded by the relatively high volume content of  $\alpha_2$  phase present in these alloys. Additionally, in high Nb containing alloys dynamic recrystallization may be impeded because of the lower diffusivity. A particular feature of the Nb-bearing alloys is also that they often contain a significant volume fraction of  $\beta$ (B2) phase, which forms a percolating substructure throughout the material [14]. It might be expected that this phase has a relatively low yield strength under hot-working conditions and carries most of the deformation. Thus, the amount of strain energy imparted into the  $\alpha_2$  and  $\gamma$  phases is relatively small so that the driving force for dynamic recrystallization in these constituents is reduced. It is tempting to speculate that the restoration of the microstructure in the  $\beta$  phase is far in advance of that in the  $\alpha_2$  and  $\gamma$  phases. In highly

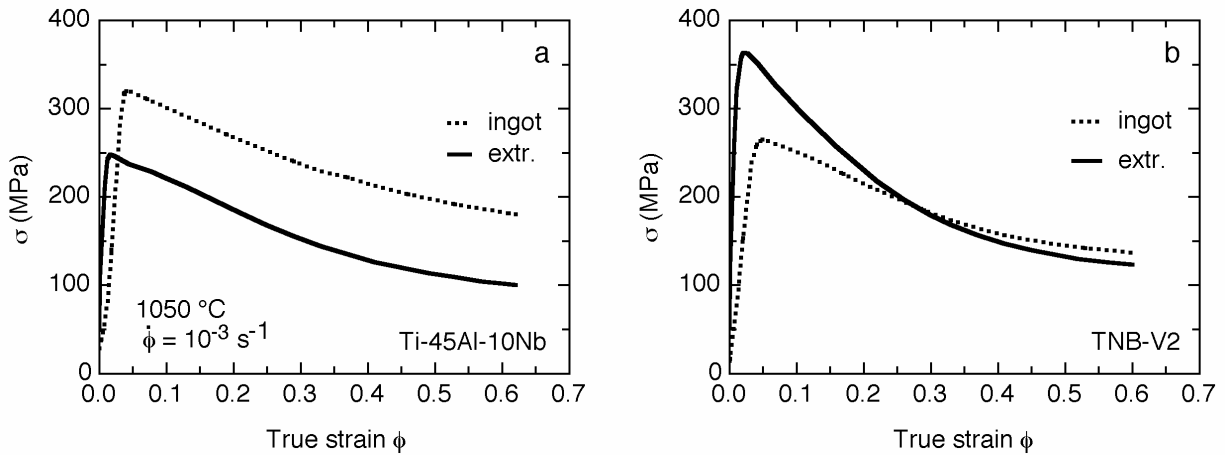


Fig. 3: Flow curves of TNB alloy measured on cylindrical compression samples of 18 mm diameter and 30 mm height tested at the conditions indicated. The true stress  $\sigma$  was calculated from the cross-sectional change under the assumption that homogeneous deformation occurred throughout the whole volume.  $\Phi = \ln(\epsilon + 1)$  is the true strain. (a) Ti-45Al-10Nb; (b) TNB-V2: Ti-45Al-Nb-C.

strained samples, along the  $\beta$  phase shear bands are often developed, which consists of very fine, equiaxed grains. Deformation may therefore preferentially occur by grain boundary sliding. Strain partitioning between the  $\beta$  phase and the other constituents of the microstructure certainly results in high internal stresses. The shear bands often completely traverse the whole sample, which in large work pieces leads to high peripheral tensile stresses and premature failure. These particular features in the hot-working of Nb-bearing alloys are demonstrated in Fig. 4 by the microstructural changes observed after intensive hot-working by combined torsion and compression [14]. This deformation behavior of the  $\beta$  phase often overshadows the low workability of high Nb containing alloys, when small test pieces are used in order to determine hot-working windows.

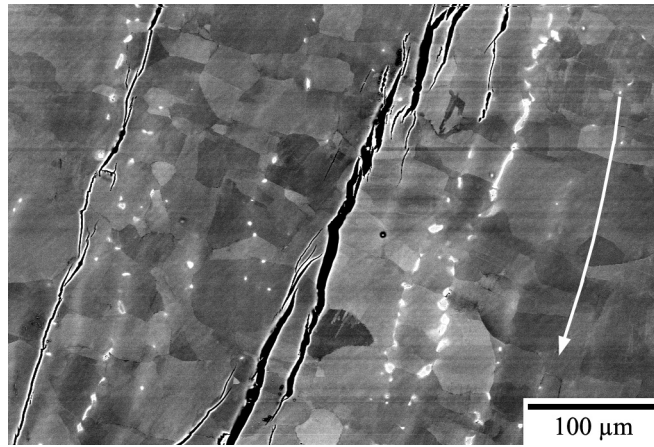


Fig. 4: Strain localization and cracking along the  $\beta$  phase during hot-working of high Nb containing alloy. BSE electron micrograph showing the microstructure in the cross-section of a sample that was torsionally deformed at  $T=1050\text{ }^{\circ}\text{C}$  through three revolutions while simultaneously compressed to  $\varepsilon=50\%$ . The arrow indicates the major shear direction occurring during torsion. TNB-V2 primary ingot-break down by extrusion in the  $\alpha$ -phase field.

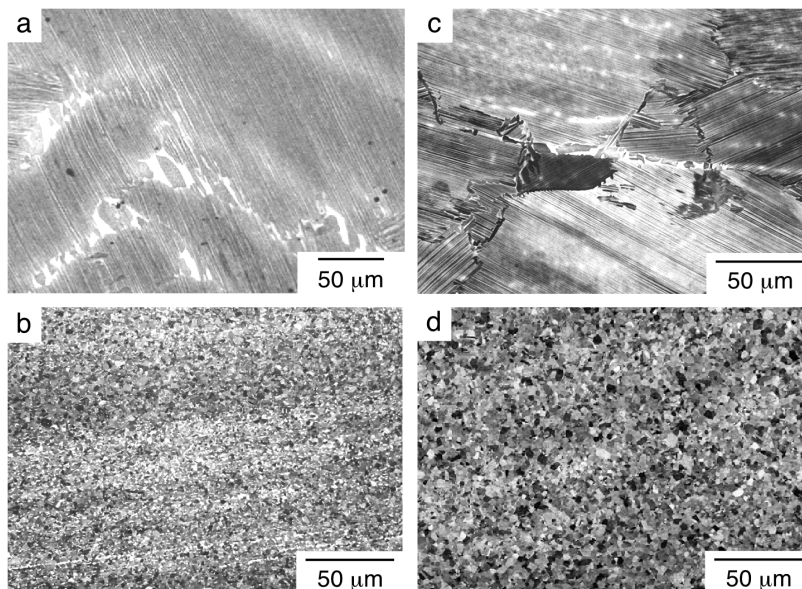


Fig. 5: BSE electron micrographs of the microstructure of a Ti-45Al-(5-10)Nb-C alloy (TNB-V2) observed after ingot break-down utilizing different variants of canned extrusion and subsequent forging. (a) Ingot material. (b) Extrusion at  $T_{\alpha}-\Delta T$  to a 10:1 reduction resulting in a banded duplex microstructure. The extrusion axis is horizontal in the micrograph. (c) Extrusion at  $T_{\alpha}+\Delta T$  to a 10:1 reduction resulting in a nearly lamellar microstructure. The extrusion direction is horizontal in (c) and (d). (d) Microstructure after extrusion as described in (b) plus subsequent forging along the extrusion direction at  $1100\text{ }^{\circ}\text{C}$  to strain  $\varepsilon=80\%$ ; the forging direction is vertical in the micrograph.

With this behavior in mind, primary ingot-break down of large ingots (>30 kg) was preferentially accomplished by canned extrusion [15]. For example, 80 kg ingots of various TNB alloys were extruded into a rectangular shape with reductions of the cross-section of 10:1. Extrusion below  $T_\alpha$  results in an equiaxed microstructure with a banded morphology (Fig. 5b), which is reminiscent of that what has been observed on conventional TiAl alloys [14,15]. These structural inhomogeneities are again associated with significant variations in the local chemical composition, which is manifested on a length scale comparable to, or slightly smaller, than that of the as-cast material. Thus, the structural inhomogeneity may in part be attributed to the elemental segregation present in the as-cast material. Extrusion performed above  $T_\alpha$  results in a nearly lamellar microstructure with a refined colony size and containing some  $\beta$  phase, which is preferentially situated at the triple points of the colonies (Fig. 5c). The microstructure of hot-worked Nb-bearing alloys exhibits particular textures, which are associated with the deformation processes occurring in the high-temperature phase field and the subsequent phase transformations  $\beta \rightarrow \alpha \rightarrow \alpha_2 \rightarrow \gamma$  [14,16].

The microstructural refinement obtained after primary extrusion significantly reduced the susceptibility to cracking in any secondary hot-working step and thus allows the material to be worked by closed-die forging or rolling techniques to produce mill products. Subsequent forging, e.g., leads to a slight increase of the grain size but otherwise very homogeneous microstructures (Fig. 5d). In this respect, it is interesting to note that the flow resistance in secondary forming processes strongly depends on the presence of precipitates. This is suggested by Fig. 3b, which demonstrates the flow curves of the TNB-V2 alloy containing a small amount of carbon. The point to note is that the as-cast specimen of this material exhibited a lower yield strength than the specimen tested after primary hot-working, in spite of the structural refinement that has been achieved by the extrusion. This is probably a consequence of precipitation reactions occurring during primary hot-working. Pre-heating of the as-cast billet at 1250 °C certainly brings carbon into solution. During extrusion and cooling the precipitates are probably heterogeneously nucleated at the newly formed grain boundaries and interfaces, which provides a very fine carbide dispersion stabilizing the microstructure and promises good creep resistance.

Within the framework of a joint BMBF-project (involving Thyssen Umformtechnik, Rolls-Royce, GfE, and GKSS) and financially supported by the German Federal Ministry for Education and Research), a complete processing technology for the production of high-pressure

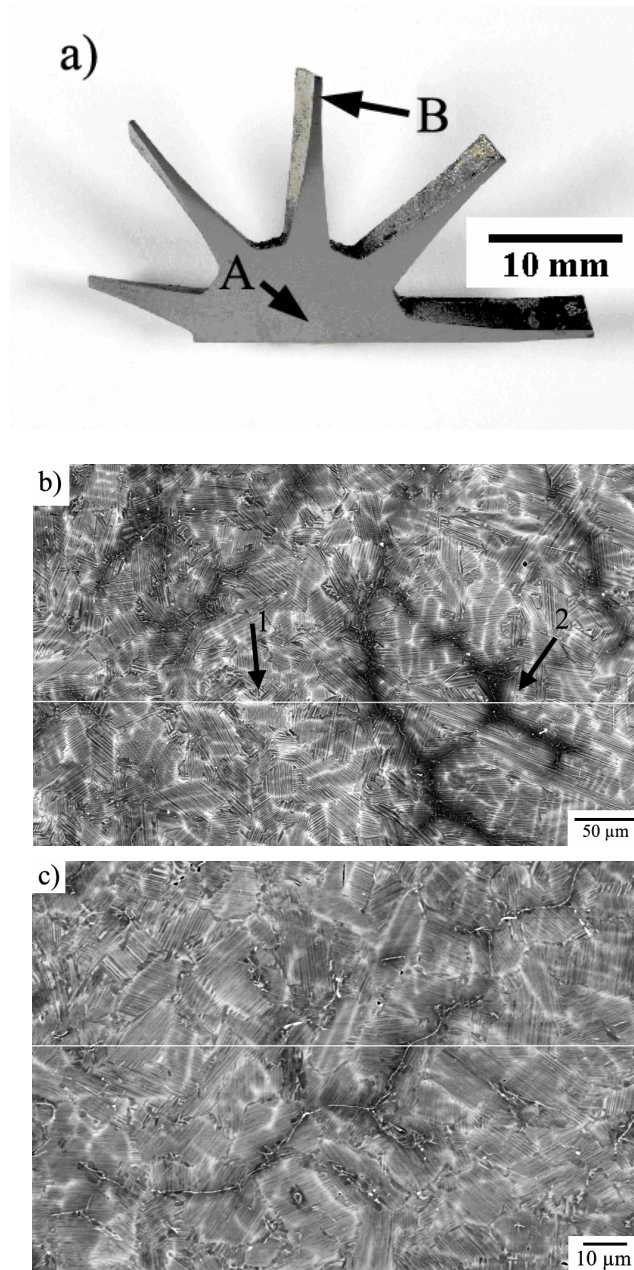


Fig. 6: Investment casting of TNB alloys. (a) Cross section of a turbocharger wheel with arrows indicating the regions where the microstructure was analyzed. Microstructure in (b) the axial and (c) the blade region of the wheel.

aero-engine blades was identified for this type of material. In spite of this progress, it must be admitted that the improvement of hot-working of TiAl alloys is still of major concern. To this end, the feasibility of torsional deformation is currently being investigated, because in such tests much higher strains can be achieved than in compression or extrusion [14].

## Investment Casting

Within a BMBF-project involving DaimlerChrysler, Access, GfE, and GKSS, the investment casting of  $\gamma$  alloys is currently being explored as a cost effective route for the mass production of automotive components. For certain applications, such as turbocharger wheels, excellent creep strength and oxidation resistance are required, which apparently can best be met with high Nb containing alloys. Furthermore, such components often have very thin walls of less than 1mm thickness. Thus, the alloy design was also focused on castability. Specifically, the alloys used should exhibit good mould filling and fine as-cast microstructures. Process development was aimed at a truly near-net shaped production; thus, there are significant constraints on the application of hot isostatic pressing or heat treatments. With these requirements in mind, different variants of TNB alloys were involved in the research program. The material was processed by induction melting and poured under centrifugal forces into pre-heated ceramic moulds. Major barriers to the application of investment casting include dimensional integrity, component cracking and surface connected porosity. Nevertheless, first trials have yielded encouraging results. There was almost no porosity found in the blade region and only very limited porosity near to the central axis, which apparently forms in the constituents of the alloy that are last to solidify. The rapid solidification that occurs in small and thin components certainly reduces segregation, refines microstructure and leads to homogeneous material consolidation. However, when compared with conventional alloys, the microstructure of the TNB castings is much finer and chemically more homogeneous, which probably arises from the change of the solidification pathway. Figure 6 demonstrates the cross section of a turbocharger wheel cast from a TNB alloy and the microstructures observed near to

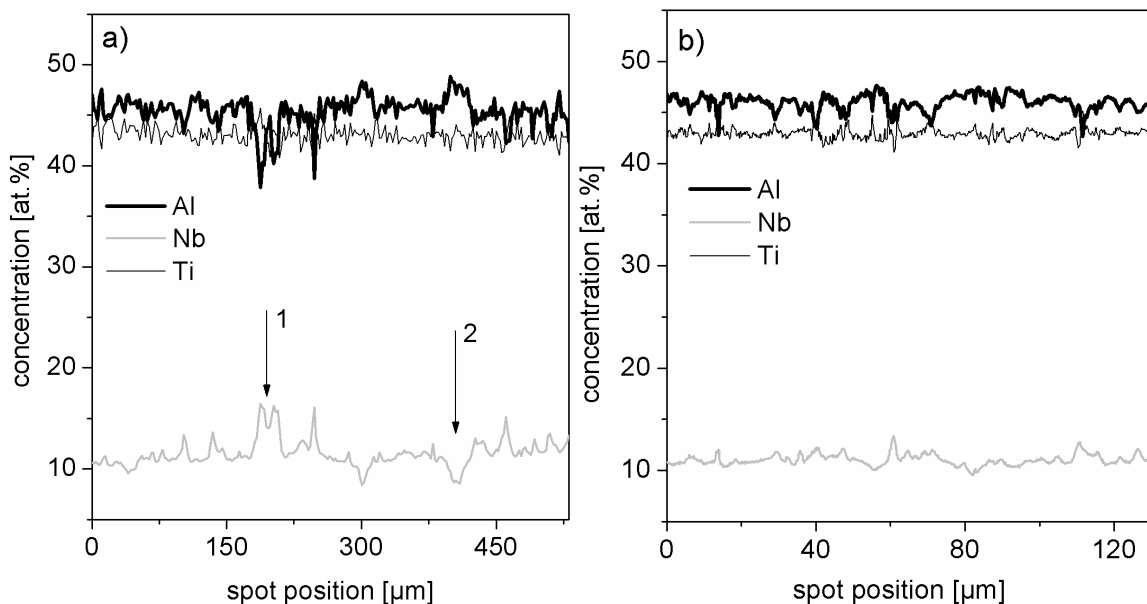


Fig. 7: Quantitative EDX analysis of the Al, Nb and Ti concentration in a turbocharger wheel. Analysis performed in (a) the axial and (b) the blade region along the white lines in Figs. 6b and 6c.

the central axis and in the blade region. The results of quantitative EDX analysis performed in the axial and blade region of the turbocharger wheel are shown in Fig. 7. It might be expected that the peritectic solidification can largely be avoided in the TNB alloy because of its low Al and high Nb content, a subject that needs further investigation.

## Mechanical Properties

The balance of properties that can be achieved with Nb-bearing alloys will be demonstrated on materials that were extruded below  $T_\alpha$  with reduction ratios of 7:1 to 14:1 [2]. The extrusions were given a final heat treatment at 1050 °C for 2 hours in air. The axis of the tensile samples was always parallel to the extrusion direction. For comparison data of investment cast samples will be presented, which were prepared by the method described above and subject to hot isostatic pressing at 1150 °C, 200 MPa for 3 hours.

### Yield Strength and Ductility

Figure 8 demonstrates load/elongation traces of tensile tests performed at 25 °C, 700 °C and 900 °C. The materials generally exhibit high yield stresses with room temperature values of 900 to 1000 MPa, which are combined with plastic elongations of 1-2 %. However, for brittle materials like TiAl, the reliability of components is most important. Figures 9a and 9b show tensile test curves of the TNB-V2 alloy with duplex microstructure, which was particularly developed for high creep resistance (see Fig. 11b). The diagram involves the minimum and maximum measured stresses and strains. It should be mentioned that no sample broke within the elastic limit. The strength variation within a given volume of such material can be analyzed in terms of Weibull statistics [17]. Figure 9c shows the values of the yield stresses  $\sigma_{0.1}$ ,  $\sigma_{0.2}$  and the fracture stress  $\sigma_f$  ranked in Weibull plots. The Weibull modulus is highest for  $\sigma_{0.1}$ , which indicates that the range of stress at which plastic flow starts is relatively narrow. The increased scatter for  $\sigma_{0.2}$  and  $\sigma_f$  can be explained with reference to Fig. 9b. The tensile test curves show a relatively wide range of work hardening after the onset of yield. Specimens that exhibited an initial high work hardening rate tended to have lower plastic elongation to failure, thus increasing the scatter of  $\sigma_{0.2}$  and  $\sigma_f$ . The microstructure of the specimen with the highest work hardening rates contained a much higher volume fraction of lamellar colonies with larger colony size than the more ductile specimens. Upon loading, in such coarse grained material, localized flow will start in favorably oriented colonies and the small plastic elongation in the pre-macro yield region may be due entirely to such non-uniform deformation. The apparently high initial rate of work hardening is then only a result of constraint stresses by localized flow. It might be expected that this localized shear can easily lead to premature failure. These findings again illustrate that a good consolidation of the microstructure is an absolute precondition in order to get a reasonable balance of mechanical properties.

### Creep Resistance

Figure 10 demonstrates the creep behavior of extruded and investment cast TNB alloys observed at 800 °C and 250 MPa. The Ti-45Al-10Nb alloy may be considered as reference material for the Nb-bearing alloys investigated in the present study. The creep resistance increases with Nb content; this is demonstrated in Fig. 11a, where two alloys containing 5 and 10 at. % Nb at otherwise constant composition were compared. The improvement can probably be attributed to a reduction of diffusivity by the high Nb additions, as discussed previously. It

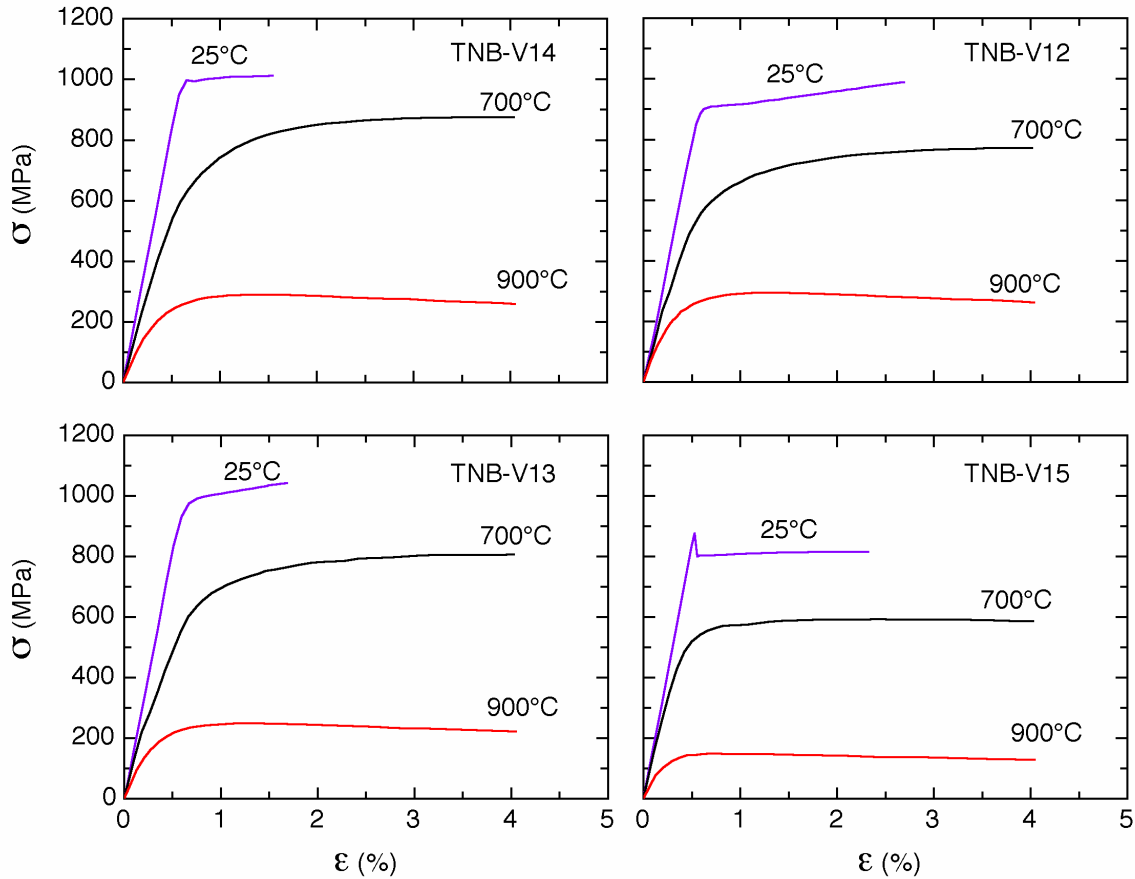


Fig. 8: Stress/strain curves obtained in tensile testing of different extruded Nb-containing alloys. The tests performed at 700 and 900 °C were stopped at  $\epsilon=4\%$ . Note the softening occurring on deformation at 900 °C, which is attributed to dynamical recrystallization.

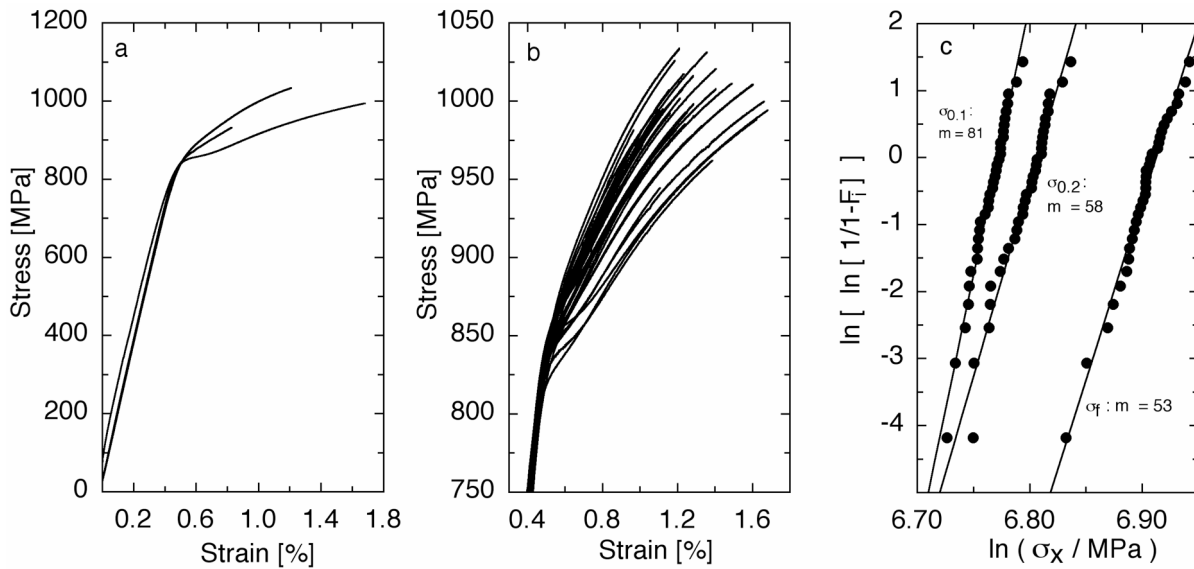


Fig. 9: Deformation behavior of the TNB-V2 alloy extruded below the  $\alpha$ -transus temperature at  $T=1230$  °C with an reduction ratio of 14:1. (a) graph showing tensile test curves obtained from selected specimens. (b) graph showing the plastic behavior of all 33 tensile tests. (c) A two-parameter Weibull plot for the stresses  $\sigma_{0.1}$ ,  $\sigma_{0.2}$  and the fracture stress  $\sigma_f$ .

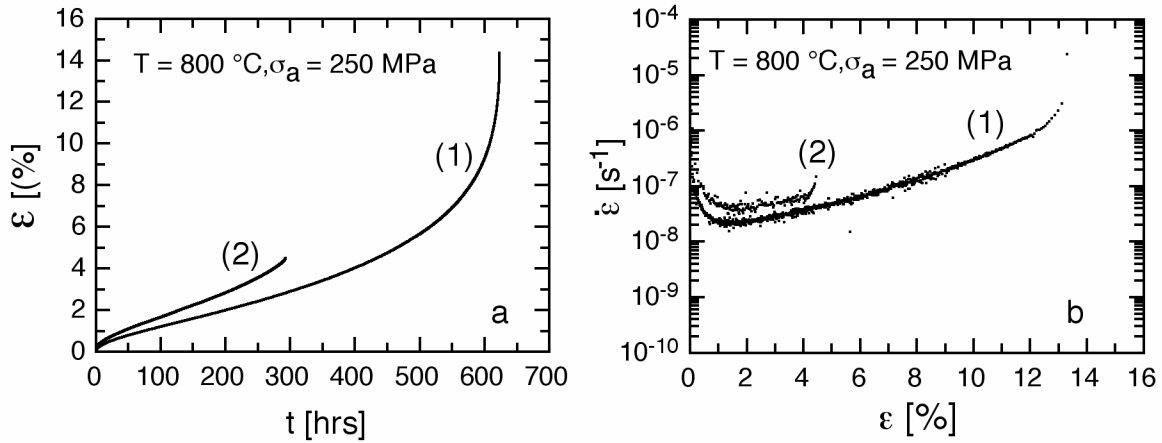


Fig. 10: Creep behavior of high Nb containing alloys. (a) Creep curves measured on extruded Ti-45Al-10Nb (1) and investment cast + HIP Ti-45Al-Nb-B-C (TNB-V5) (2); (b) variation of the strain rate  $\dot{\epsilon}$  with strain  $\epsilon$  determined from the creep curve shown in (a).

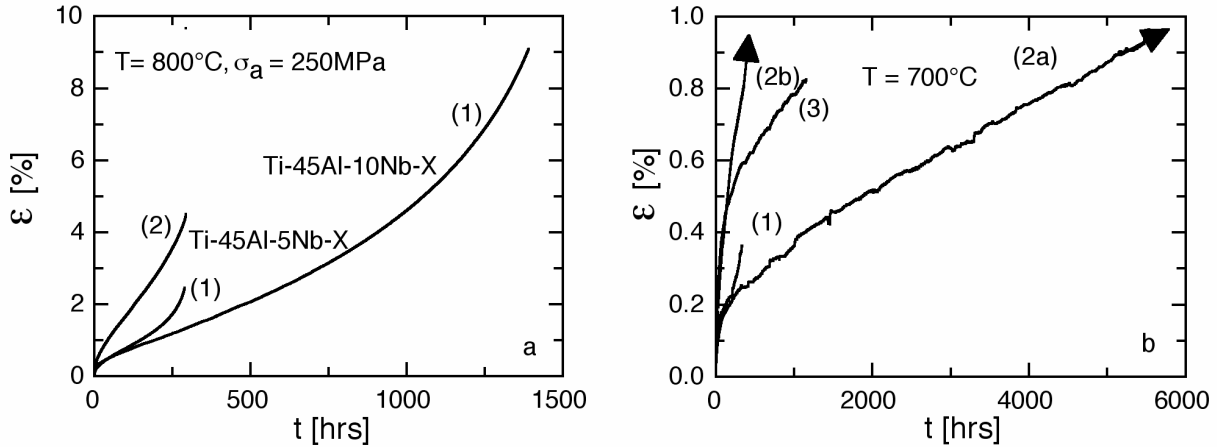


Fig. 11: Effect of processing and alloy composition on the creep behavior of TNB alloys. (a) Influence of Nb content, (1) extruded alloys of composition Ti-45Al-Nb-B-C (TNB-V5), and Ti-45Al-Nb-B-C, both with a similar duplex microstructure, (2) investment cast + HIP Ti-45Al-5Nb-B-C (TNB-V5), with nearly lamellar microstructure. (b) Effect of carbide precipitates on creep resistance. Comparison of the carbon-free reference material with carbon doped material: (1) Ti-45Al-10Nb,  $\sigma_a=300$  MPa, (2a) Ti-45Al-Nb-C (TNB-VL),  $\sigma_a=300$  MPa, (2b) Ti-45Al-Nb-C (TNB-V2),  $\sigma_a=500$  MPa, note the low creep rate of  $\dot{\epsilon}=6 \times 10^{-9} \text{ s}^{-1}$ , (3) investment cast + HIP Ti-45Al-Nb-B-C (TNB-V5),  $\sigma_a=300$  MPa.

should be noted that the extruded material (1) with duplex microstructure exhibits superior creep resistance, when compared with its investment cast counterpart (2) with nearly lamellar microstructure. As already mentioned, this is probably a consequence of the precipitation reactions occurring during extrusion, which apparently stabilize the fine microstructure. Figure 11b demonstrates the synergistic effects that can be achieved by the implementation of carbide precipitates in high Nb containing alloys. The carbon additions lead to a significant improvement of the creep resistance, when compared with the undoped reference material Ti-45Al-10Nb. The improvement can be attributed to an increase of the glide and climb resistance

of the dislocations by the presence of perovskite  $Ti_3AlC$  or H-phase  $Ti_2AlC$  precipitates. As has been discussed before, a significant part of the precipitates is probably heterogeneously nucleated at the mismatch structures of the lamellar interfaces and grain boundaries so that the microstructure is stabilized. Addition of elements that are known to stabilize the  $\beta$  phase seems to be harmful for the creep resistance of this class of alloys. In particular, it might be speculated that in Cr containing alloys a significantly higher volume fraction of  $\beta$  phase is formed, that is apparently detrimental for the structural stability and gives rise to the strong acceleration of the creep rate almost from the beginning of the test [18].

With this problem in mind, optimized compositions of precipitation hardened alloys could be identified that represent a high potential as creep resistant material. This is manifested by the fact that even at 700 °C and creep stresses of  $\sigma_a=500$  MPa appreciable low deformation rates of  $\dot{\epsilon}=6 \times 10^{-9} s^{-1}$  occur. Figure 12 demonstrates a density corrected Larson-Miller plot of the creep data of the investment cast TNB-V5 alloy, that also contains data for the well-established high-temperature alloy René 80 and conventional TiAl alloys. The comparison indicates that this novel class of high-strength TiAl alloys can be an attractive alternative to the nickel-base superalloys in the intermediate temperature interval of 700-800 °C. The adequate collection of data for extruded TNB alloys was provided in [20].

### Conclusions

TiAl alloys containing 5-10 at.% Nb and subjected to precipitation hardening exhibit several desired attributes for high-temperature structural applications. Wrought and investment cast alloys of this type exhibit outstanding strength and creep resistance combined with good oxidation resistance, which give them the potential to expand the service range of conventional TiAl alloys and to be an attractive alternative to the heavier nickel-base superalloys in intermediate ranges of stress and temperature. The future and promise of these novel alloys and

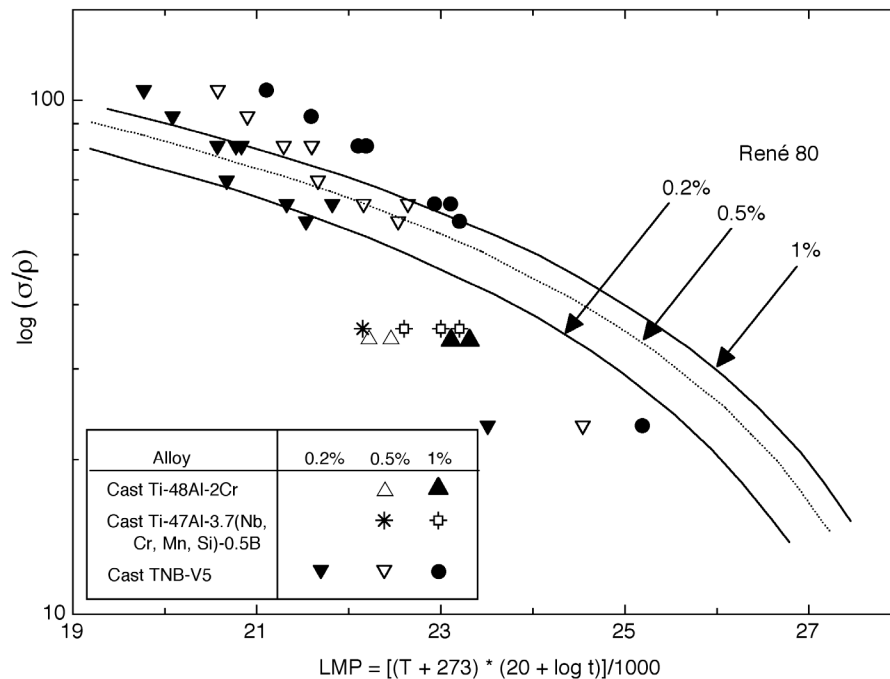


Fig. 12: Density corrected Larson-Miller plot for René 80 and different cast TiAl alloys. The alloy TNB-V5 represents a precipitation hardened high niobium containing TiAl alloy.

manufacturing of components lies in innovative processing methods designed to achieve better performance. Specifically, substantial improvements are required in ingot quality and hot-working procedures to obtain homogeneous and defect-free material with desired microstructures.

### Acknowledgements

The authors acknowledge helpful discussions and continuous support from Ms. E. Schröder, Ms. E. Tretau, U. Fröbel, St. Eggert, U. Lorenz, and J. Müllauer.

### References

1. J.D.H. Paul, F. Appel and R. Wagner, *Acta Mater.* 46, 1075 (1998).
2. F. Appel, M. Oehring and R. Wagner, *Intermetallics* 8, 1283 (2000).
3. F. Appel, M. Oehring, J.D.H. Paul, and U. Lorenz, in: *Structural Intermetallics 2001*, eds. K.J. Hemker, D.M. Dimiduk, H. Clemens, R. Darolia, H. Inui, J.M. Larsen, V.K. Sikka, M. Thomas, J.D. Whittenberger (TMS, Warrendale, PA, 2001), p. 63.
4. S.-C. Huang, in: *Structural Intermetallics*, eds. R. Darolia, J.J. Lewandowski, C.T. Liu, P.L. Martin, D.B. Miracle, M.V. Nathal (TMS, Warrendale, PA, 1993), p. 299.
5. G. Chen, W. Zhang, Y. Wang, J. Wang, and Z. Sun, in: *Structural Intermetallics*, eds. R. Darolia, J.J. Lewandowski, C.T. Liu, P.L. Martin, D.B. Miracle, M.V. Nathal (TMS, Warrendale, PA, 1993), p. 319.
6. G.L. Chen, W.J. Zhang, Z.C. Liu, S.J. Li, and Y-W. Kim, in: *Gamma Titanium Aluminides 1999*, eds. Y-W. Kim, D.M. Dimiduk and M.H. Loretto (TMS, Warrendale, PA, 1999), p. 371.
7. C.J. Rossouw, C.T. Forwood, M.A. Gibson, and P.R. Miller, *Phil. Mag.* A74, 77 (1996).
8. C. Woodward, S.A. Kajihara, S.I. Rao, and D.M. Dimiduk, in: *Gamma Titanium Aluminides 1999*, eds. Y-W. Kim, D.M. Dimiduk and M.H. Loretto (TMS, Warrendale, PA, 1999), p.49.
9. F. Appel in: *Advances in Twinning*, eds. S. Ankem, C.S. Pande (TMS, Warrendale, PA, 1999), p. 171.
10. Chr. Herzig, T. Przeorski, M. Friesel, F. Hisker, and S. Divinski, *Intermetallics* 9, 461 (2001).
11. C. Buque and F. Appel, *Z. Metallkd.* 93, 784 (2002).
12. C. Buque and F. Appel, *Gamma Titanium Aluminides 2003*, eds. Y-W. Kim et al.
13. R.M. Imayev, G.A. Salishchev, V.M. Imayev, M.R. Shagiev, A.V. Kuznetsov, F. Appel, M. Oehring, O.N. Senkov, and F.H. Froes, in: *Gamma Titanium Aluminides 1999*, eds. Y-W. Kim, D.M. Dimiduk and M.H. Loretto (TMS, Warrendale, PA, 1999), p. 565.
14. F. Appel, M. Oehring, J.D.H. Paul, Ch. Klinkenberg, and T. Carneiro, *Intermetallics*, in print.
15. U. Brossmann, M. Oehring and F. Appel, in: *Structural Intermetallics 2001*, eds. K.J. Hemker, D.M. Dimiduk, H. Clemens, R. Darolia, H. Inui, J.M. Larsen, V.K. Sikka, M. Thomas, J.D. Whittenberger (TMS, Warrendale, PA, 2001), p. 191.
16. H.-G. Brockmeier, M. Oehring, U. Lorenz, H. Clemens, and F. Appel, *Metall. Mater. Trans. A*, in print.
17. J.D.H. Paul, R. Hoppe, M. Oehring, and F. Appel, in: *Gamma Titanium Aluminides 2003*, eds. Y-W. Kim et al. (TMS, Warrendale, PA), in print.
18. F. Appel, J.D.H. Paul, M. Oehring, U. Fröbel, and U. Lorenz, *Metall. Mater. Trans. A*, in print.
19. J.G. Wang and T.G. Nieh, *Intermetallics* 8, 737 (2000).
20. F. Appel, J.D.H. Paul, M. Oehring, and C. Buque, in: *Gamma Titanium Aluminides 2003*, eds. Y-W. Kim et al. (TMS, Warrendale, PA) in print.